Tracking the precession of compact binaries from their gravitational-wave signal

Patricia Schmidt,[1,2] Mark Hannam,[1,2] Sascha Husa,[3] and P. Ajith[4,5]

[1]*School of Physics and Astronomy, Cardiff University, Queens Building, CF24 3AA, Cardiff, United Kingdom*
[2]*Gravitational Physics, Faculty of Physics, University of Vienna, Boltzmanngasse 5, A-1090 Vienna, Austria*
[3]*Departament de Física, Universitat de les Illes Balears, Crta. Valldemossa km 7.5, E-07122 Palma, Spain*
[4]*LIGO Laboratory, California Institute of Technology, Pasadena, California 91125, USA*
[5]*Theoretical Astrophysics, California Institute of Technology, Pasadena, California 91125, USA*

(Received 17 December 2010; published 29 July 2011)

We present a simple method to track the precession of a black-hole-binary system during the inspiral, using only information from the gravitational-wave (GW) signal. Our method consists of locating the frame from which the magnitudes of the ($\ell = 2$, $|m| = 2$) modes are maximized, which we denote the ''quadrupole-aligned'' frame. We demonstrate the efficacy of this method when applied to waveforms from numerical simulations. In the test case of an equal-mass nonspinning binary, our method locates the direction of the orbital angular momentum to within $(\Delta\theta, \Delta\varphi) = (0.05°, 0.2°)$. We then apply the method to a $q = M_2/M_1 = 3$ binary that exhibits significant precession. In general, a spinning binary's orbital angular momentum $\mathbf{L}$ is *not* orthogonal to the orbital plane. Evidence that our method locates the direction of $\mathbf{L}$ rather than the normal of the orbital plane is provided by comparison with post-Newtonian results. Also, we observe that it accurately reproduces similar higher-mode amplitudes to a comparable non-precessing binary, and that the frequency of the ($\ell = 2$, $|m| = 2$) modes is consistent with the ''total frequency'' of the binary's motion. The simple form of the quadrupole-aligned waveform may be useful in attempts to analytically model the inspiral-merger-ringdown signal of precessing binaries, and in standardizing the representation of waveforms for studies of accuracy and consistency of source modelling efforts, both numerical and analytical.

DOI: 10.1103/PhysRevD.84.024046 PACS numbers: 04.25.dg, 04.25.Nx, 04.30.Db, 04.70.Bw

I. INTRODUCTION

Black-hole-binary mergers are expected to be key sources for gravitational-wave (GW) astronomy [1]. Accurate theoretical models of the GW signal are necessary both to detect these sources and to determine their physical parameters and their location in the universe. The GW signal can be calculated from the inspiral by analytic approximation techniques [2,3], and from the merger and ringdown by numerical simulations in full general relativity [4–7].

Numerical simulations produce waveforms for only discrete points in the parameter space of binary configurations, but significant progress has been made in synthesizing information from post-Newtonian (PN) and effective-one-body methods, numerical relativity (NR), and perturbation theory, to produce analytic models of the complete inspiral-merger-ringdown signal over some regions of the parameter space. Most models to date treat nonspinning binaries [8–18], or binaries in which the black-hole spins do not precess [19–21] (although there has been one first attempt at a precession model [22]).

Precession adds a number of complications. When the spins are not parallel to the orbital angular momentum their orientation varies with time, as does the orbital angular momentum itself; the orbital plane precesses. The precession of the spins and of the orbital plane each introduce modulations into the GW amplitude, oscillations into the GW frequency, and variations in the distribution of signal power across different harmonics of the waveform. All of these complicate efforts to produce an analytic model of precessing-binary waveforms. In addition, they make it difficult to uniquely characterize the wave signal. For example, the total phase of the dominant mode of the signal depends on the initial orientation of the orbital plane. This makes it difficult to determine whether two waveforms were produced by the same binary configuration, or to compare independent numerical simulations, a task that is relatively simple for nonprecessing, noneccentric binaries [23–25].

We propose a method to put a precessing-binary waveform into a particularly simple form. The method is based on finding a preferred time-dependent coordinate system for the GW signal, which tracks the precession during the inspiral.

Gravitational-wave signals are most conveniently expressed in terms of spherical harmonics of spin-weight $s = -2$, $Y^s_{lm}(\theta, \varphi)$, where (θ, φ) are the standard polar coordinates on the unit sphere. The dominant modes are the quadrupole modes, where ($\ell = 2$, $m = \pm 2$). If the system is rotated, the modes of a particular ℓ mix among each other according to the transformation law described in Appendix A.

As can be seen from the quadrupole formula, binary systems emit GWs predominantly in the direction orthogonal to the orbital plane. Correspondingly, if our system is oriented such that this direction is along the z-axis, then we

expect that the dominant signal is given by the ($\ell = 2$, $|m| = 2$) spherical harmonics of the wave. The modes $|m| = 1$ vanish when the two black holes can be exchanged by symmetry, and $m = 0$ is a nonoscillating mode related to memory effects, see, e.g., [26,27]. If we choose different (rotated) coordinates (θ', φ') to define a new basis $Y^s_{lm}(\theta', \varphi')$, then mode mixing will complicate the spherical harmonic description of the signal, and, for example, even an equal-mass nonspinning binary will exhibit nonvanishing $|m| = 1$ modes. We illustrate this effect in Sec. IV A.

Therefore, we can determine a preferred direction *from the wave signal alone* by finding the orientation that maximizes the ($\ell = 2$, $|m| = 2$) modes. This is the method that we will discuss in this paper, and we will refer to waveforms that are given in terms of spherical harmonics that are aligned with this direction as ''quadrupole-aligned'' waveforms.

In a precessing system there are two contributions to the frequency of the binary motion: the frequency of the motion about the orbital-plane axis, $\omega_{\rm orb}$, which increases during a noneccentric inspiral as a monotonic function, and the frequency due to the precessional motion, which oscillates as a function of time. The total frequency of the motion is $\omega = \omega_{\rm orb} - \dot{\varphi}\cos\theta$, where θ is the inclination of the normal to the orbital plane from the z-axis, and φ is the rotation of the normal about the z-axis in the xy plane. (This corresponds to the result in Eq. (3.10) in [28].) In a kinematical description of the binary, these two frequencies together prescribe the bodies' acceleration, which is the dominant source of gravitational radiation. One of the properties we expect from our quadrupole-aligned waveform is that during the inspiral the frequency of the ($\ell = 2$, $|m| = 2$) modes will to a good approximation satisfy the relation

$$\omega_{22} = 2(\omega_{\rm orb} - \dot{\varphi}\cos\theta). \tag{1.1}$$

Our main results are that (1) we can determine the quadrupole-aligned direction from the GW signal to high accuracy (within a fraction of a degree during most of the inspiral), and (2) the GW signal is indeed far simplified, see, in particular, Fig. 10 of the GW frequency before and after our (2, 2)-maximization procedure, where the final frequency does approximately satisfy Eq. (1.1). In addition, we show that the GW signal is emitted in the direction of the orbital angular momentum of the binary, which is *not* in general perpendicular to the orbital plane. We illustrate this effect with an example from PN theory, where it can be seen explicitly that the effective orbital angular momentum is not parallel to the naive Newtonian angular momentum.

In Sec. II we describe our numerical methods and numerical simulations, and in Sec. III provide details of our algorithm to find the orbital-angular-momentum direction from the GW signal. The results of our method are presented in Sec. IV, where we verify our method using a simple test case of an equal-mass nonspinning binary, and then apply the method to an unequal-mass spinning binary that undergoes significant precession. We discuss these results and prospects for future work in Sec. V.

II. NUMERICAL METHODS AND SIMULATIONS

We performed numerical simulations with the BAM code [29,30]. The code starts with black-hole-binary puncture initial data [31,32] generated using a pseudospectral elliptic solver [33], and evolves them with the χ-variant of the moving-puncture [5,6,34] version of the Baumgarte-Shapiro-Shibata-Nakamura [35,36] formulation of the 3 + 1 Einstein evolution equations. Spatial finite-difference derivatives are sixth-order accurate in the bulk [30], Kreiss-Oliger dissipation terms converge at fifth order, and a fourth-order Runge-Kutta algorithm is used for the time evolution. The GWs emitted by the binary are calculated from the Weyl scalar Ψ_4, and the details of our implementation of this procedure are given in [29]. See, e.g., [37] for a recent extensive parameter study of nonprecessing binaries that uses the same numerical code and general setup.

In each simulation, the black-hole punctures are initially a coordinate distance D apart, and are placed on the y-axis at $y_1 = -qD/(1 + q)$ and $y_2 = D/(1 + q)$, where $q = M_2/M_1$ is the ratio of the black-hole masses in the binary, and we always choose $M_1 < M_2$. The masses M_i are estimated from the Arnowitt-Deser-Misner mass at each puncture, according to the method described in [31]; see also the Appendix of [37] and the discussion in [38]. The Bowen-York punctures are given momenta $p_x = \mp p_t$ tangential to their separation vector, and $p_y = \pm p_r$ towards each other. The latter momentum component accounts for the (initially small) radial motion of the black holes as they spiral together. Initial parameters for low-eccentricity inspiral were produced using integrations of the PN equations of motion, as described in [37,39].

The eccentricity is measured with respect to the frequency of the orbital motion, as in all of our past work on eccentricity removal [37,39–41], and also discussed in [42,43] and references therein. The eccentricity is estimated as the extrema of $e_\omega(t) = (\omega(t) - \omega_{QC}(t))/(2\omega_{QC}(t))$, where ω is the frequency of the ($\ell = 2$, $m = 2$) mode of the waveform, and $\omega_{QC}(t)$ is an estimate of the frequency evolution for a noneccentric binary, calculated by a smooth curve fit through the numerical data.

The grid setup is similar to that used in [29], although in the precessing-binary simulation the number of points on each refinement level is varied to achieve greater wave-extraction accuracy. The base configuration is of the form $\chi_{M\eta=2}[l_1 \times N{:}l_2 \times 2N{:}6]$. This indicates that the simulation used the χ variant of the moving-puncture method, l_1 moving nested mesh-refinement boxes with a base value of N^3 points surround each black hole, and l_2 fixed nested boxes with $(2N)^3$ points surround the entire system, and

there are six mesh-refinement buffer points. The η parameter in the Baumgarte-Shapiro-Shibata-Nakamura system is $M\eta = 2$.

The resolution around the puncture is denoted by $M_1/h_{\rm min}$, which is the resolution with respect to the *smaller black hole*, M_1. The puncture of the second black hole will have the same numerical resolution, but if the black hole is bigger, $M_2 > M_1$, then it will effectively be better resolved. In unequal-mass cases, different numbers of refinement levels can be used around each black hole, so that the larger black hole need not be unnecessarily well-resolved, which would slow down the code. Far from the sources, the meaningful length scale is the total mass of the binary, $M = M_1 + M_2$, and so the resolution on the coarsest level is given by $h_{\rm max}/M$.

We consider two configurations. The first is an equal-mass nonspinning binary, using the same setup as first described in [44]. The initial separation is $D = 12M$, and the binary completes about nine orbits before merger. To test our orbital-plane tracking algorithm (which we will describe in Sec. III), we performed a new simulation of this case in which the orbital plane was first rotated by 10° about the y-axis (tilt), and then around the z-axis by 25° (twist). For this simulation the grid configuration was the same as the $N = 64$ simulation in [44] (although of course with a full grid, and no symmetries applied). For reference, this grid was characterized by $N = 64$, $l_1 = l_2 = 5$, $M_1/h_{\rm min} = 21.3$, $h_{\rm max} = 12M$, and the extent of the grid was $x_{i,\rm max} = 774M$; the resolution on the wave-extraction level was $h_{\rm ex} = 1.5$.

The second configuration is a precessing binary with mass ratio $q = 3$, where the larger black hole has spin $S_2/M_2^2 = 0.75$. In the calculation of the initial parameters, the spin is directed perpendicular to the orbital angular momentum when the binary is at a separation of $D = 30M$. The configuration is evolved using the PN equations of motion until about $D = 10M$, and the momenta read off from the PN evolution at a point where the point particles pass through the xy plane. A low-resolution simulation is performed with these initial parameters, and then an additional iteration is performed to further reduce the eccentricity; more details of a refined version of this procedure will be presented in [45]. This leads to the parameters given in Table I. For this simulation $N = 112$. The number of moving levels is $l_1 = 4$ around the large black hole, and $l_1 = 5$ around the small black hole. The number of fixed levels is $l_2 = 8$, but the sizes of the fixed boxes are of varying sizes, with 448^3 points on the wave-extraction level, and with $h_{\rm ex} = 0.46M$. The resolution at the puncture is $M_1/h_{\rm min} = 35.7M$, and the resolution is $h_{\rm max} = 29.26M$ on the coarsest level that extends to $x_{i,\rm max} = 1653M$, and so the outer boundary is causally disconnected from the source over the course of the simulation.

Some key physical properties of the simulations are given in the last three rows of Table I: the estimate of the eccentricity of the binary, the time when the GW signal reaches its peak amplitude, and the number of GW cycles up until that time (excluding the initial pulse of junk radiation).

TABLE I. Parameters for the two configurations that we consider in this paper: the equal-mass nonspinning case, and the $q = 3$ precessing-spin case. (For the rotated equal-mass nonspinning case, the momenta are $\mathbf{p}_i = \mp\{0.07567, 0.03588, 0.01477\}$.) The lower rows indicate some physical properties of the configuration: the initial eccentricity e, the time until the peak amplitude of the $\ell = 2$, $m = 2$ mode, and the number of GW cycles up to that time.

q	1	3
m_i	{0.488278, 0.488278}	{0.47790, 1.02343}
$\mathbf{S}_1$	{0, 0, 0}	{0, 0, 0}
$\mathbf{S}_2$	{0, 0, 0}	{−1.048, 1.197, 0.560}
$\mathbf{x}_1$	{0, 6, 0}	{0, 15.0478, 0}
$\mathbf{x}_2$	{0, −6, 0}	{0, −5.0159, 0}
D/M	12.00	10.05
$\mathbf{p}_x$	∓0.085035	∓0.126292
$\mathbf{p}_y$	±0.000537	∓0.00139578
$\mathbf{p}_z$	0	±0.0696932
e	0.0016	0.0015
$t_{\rm peak}/M$	1940	1271
$N_{\rm cycles}$	19	14

III. MAXIMIZATION PROCEDURE ALGORITHM

The Weyl scalar Ψ_4 as calculated from the numerical code is decomposed into standard spin-weighted spherical harmonics (see [29] for our implementation). We expect that if the orbital angular momentum $\mathbf{L}$ of the binary is parallel to the z-axis in the numerical simulation, then the GW signal will be dominated by the ($\ell = 2$, $|m| = 2$) modes. We also expect that the coefficient of the ($\ell = 2$, $|m| = 2$) modes will be maximal in this case; for any other orientation of the orbital angular momentum, the ($\ell = 2$, $|m| = 2$) modes will be weaker.

Given the $\ell = 2$ modes $\Psi'_{4,2m}$ from the numerical code, we can rotate the frame to any other orientation using the transformation described in Appendix A, to produce the corresponding $\Psi_{4,2m}$ in that frame. We locate the direction of the orbital angular momentum by searching over a range of the Euler angles (β, γ) to find a global maximum in $\Psi_{4,22}$ at each time step.

The procedure in practice is as follows. We start our analysis after the passage of the pulse of junk radiation. Since we extract the GW signal at either $R_{\rm ex} = 90M$ or $R_{\rm ex} = 94M$, we take the start time to be at about $t = 150M$ or $t = 200M$, respectively. We produce a first guess of the direction of $\mathbf{L}$ from the locations and velocities of the black-hole punctures at that time. This provides a guess (β_0, γ_0) of the Euler angles by which to rotate the system. Given this initial guess, we then search over a range of

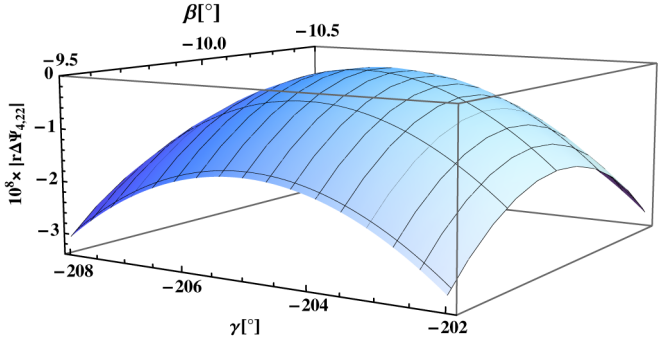

FIG. 1 (color online). Profile of the magnitude of $\Psi_{4,22}$ as the system is rotated by the Euler angles β and γ, shown relative to the maximum value. The example is taken from one time step ($t = 562M$) of the rotated equal-mass nonspinning case discussed in Sec. IV A. Note that the maximum is clearly defined, which in this case is at $(\beta, \gamma) = (-10°, -205°)$.

$(\beta, \gamma) = (\beta_0 \pm 10°, \gamma_0 \pm 10°)$ with an angular resolution of 0.1°, and find the angle for which the function $\sqrt{|\Psi_{4,22}|^2 + |\Psi_{4,2-2}|^2}$ has a maximum. In our test cases, where the orientation is constant, this procedure is trivial, but in general this first guess may not be very accurate. In particular, it does not take into account the time lag from the source to the GW extraction sphere. However, we do not expect the system to precess by as much as 10° over $\sim 100M$ of evolution. We also know that the Newtonian orbital angular momentum $\mathbf{L_N}$ calculated from the puncture motion is not in general parallel to the direction that maximizes the ($\ell = 2$, $m = 2$) mode, but we do not expect the deviation to be larger than a few degrees; we will discuss this point further at the end of Sec. IV.

For subsequent times, we use the angles from the previous time step as the first guess, and now search over the smaller range of ±3° in each angle. We locate the maximum in $\sqrt{|\Psi_{4,22}|^2 + |\Psi_{4,2-2}|^2}$ with a quadratic curve fit through the data from the search.

At all times we find a clear maximum in the amplitude of $\Psi_{4,22}$ as a function of the rotation angles. An example is given in Fig. 1, based on one time step of the rotated equal-mass nonspinning case presented in Sec. IV A.

IV. NUMERICAL RESULTS

A. Test case: equal-mass nonspinning binary

In order to test our maximization procedure, we consider two simulations of an equal-mass nonspinning binary. In one, a reference case, the orbital angular momentum is oriented parallel to the z-axis, and so the waveform is already in the quadrupole-aligned frame. The simulation starts at $D = 12M$ and covers about nine orbits before merger.

For the second simulation we change the orientation of the orbital plane. It is first rotated about the y-axis by 10°, and then around the z-axis by 25°. The motion of the punctures in both the reference and rotated cases is shown in Fig. 2. The modes of $\Psi_{4,\ell m}$ are now mixed, and the power in the $\Psi_{4,22}$ mode is distributed amongst the other ($\ell = 2$) modes. This can be seen in Fig. 3. In the reference case (denoted by $\tilde{\Psi}_{4,\ell m}$), the ($\ell = 2$, $m = 1$) mode is zero by symmetry, and the ($\ell = 2$, $m = 0$) mode is dominated by numerical noise. In the rotated case, however, both subdominant modes have become significant. Note that oscillations are visible in the ($\ell = 2$, $m = 0$) mode amplitude because it is a purely real function.

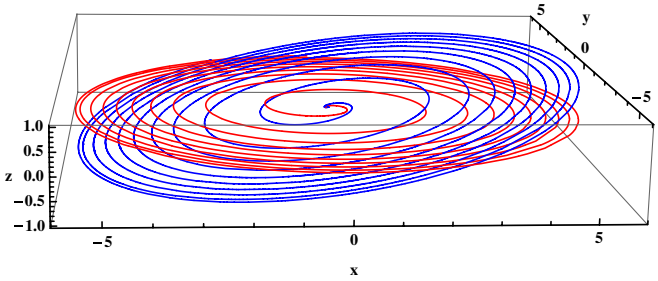

FIG. 2 (color online). Motion of one black-hole puncture for the reference and rotated cases. The orbital planes are related by a rotation about the y-axis of 10°, and about the z-axis of 25°.

We now want to see if our maximization procedure be applied to the waveform from the rotated configuration, to recover the waveform from the reference configuration. In our procedure we search for a rotation of the system by the Euler angles (β, γ) such that the coefficients of the ($\ell = 2$, $|m| = 2$) modes are maximized. If the method works, we will recover the reverse angles $(-10°, -205°)$.[1]

Figure 4 shows the error in the determination of the Euler angles. The maximization procedure was applied from $t = 150M$, after the burst of junk radiation has passed, through to $t = 2000M$, which is late in the ringdown phase. Up until about $t = 500M$ the waveform is rather noisy, and so the error in β can be as large as 1°, and in γ the error is up to 4°. During most of the inspiral, however, when the wave signal is clean, the error in β is below 0.05°, and the error in γ is below 0.2°, and even during ringdown (when the waveform amplitude is falling exponentially), the angles are determined to within $\pm(0.5°, 2.0°)$.

Note that during the merger and ringdown we do not expect the method to necessarily work. The dominance of the ($\ell = 2$, $|m| = 2$) modes, which we expect during inspiral, may not hold through merger. In addition, the signal during ringdown is no longer a superposition of spin-weighted spherical harmonics, but of spin-weighted *spheroidal* harmonics [46]. In this test case we find that our method continues to work well through merger and

[1]The Euler angle to reverse the twist is −205° due to the freedom in performing the rotation about the z-axis clockwise or counterclockwise.

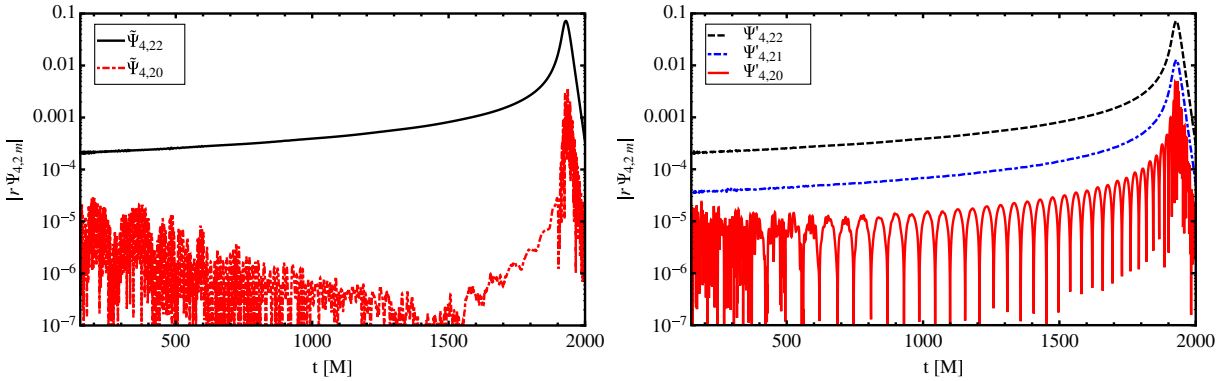

FIG. 3 (color online). The left panel shows the amplitude of the $\tilde{\Psi}_{4,2m}$ modes for the reference case. The $\ell = 2$, $m = 1$) mode is zero by symmetry, and we see that the ($\ell = 2$, $m = 0$) mode is much smaller than the dominant mode, and is essentially noise during most of the inspiral. The right panel shows the corresponding amplitudes for the rotated case. We now see that both subdominant modes have become significant. The amplitude of the ($\ell = 2$, $m = 0$) mode is oscillatory because it is a purely real function; see text for more details.

ringdown, but this will not be true in general, as we will see later.

The magnitudes of the $\ell = 2$ modes in the quadrupole-aligned waveform agree well with those in the reference case. The ($\ell = 2$, $|m| = 2$) modes agreed within numerical error in the raw data, and the ($\ell = 2$, $|m| = 1$) modes, which should be zero by symmetry, were reduced by 3 orders of magnitude, to a level that would generally be regarded as noise. During the inspiral, for example, $|\Psi_{4,21}|$ was reduced from $\sim 10^{-4}$ to $\sim 10^{-7}$.

These results demonstrate that our method works, and give us an indication of the error bounds. We expect that in general the errors will depend on the orientation angles of the binary, and will be worse when the angles are small. In these cases the subdominant modes will be smallest, and therefore will be resolved with less accuracy in the numerical code, and will then contribute more noise to the waveform in the rotated frame. However, we will take the errors from this example as the basis for our error bounds in other applications of our method.

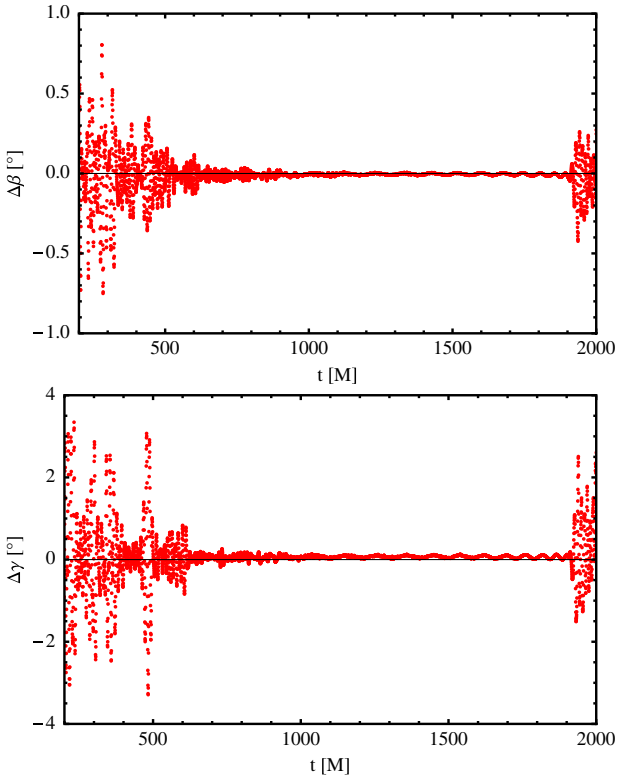

FIG. 4 (color online). Error in the angles for the tilt (β) and twist (γ) of the orbital plane, as determined by the maximization procedure.

B. Precessing binary

Having shown that the maximization procedure works for the equal-mass nonspinning test case, where the orientation of the orbital plane is known, we now apply the method to a precessing binary. The configuration we have chosen has a mass ratio of $q = M_2/M_1 = 3$, the larger black hole has a spin of $S_2/M_2^2 = 0.75$, and the spin initially lies in the orbital plane, i.e., perpendicular to the Newtonian orbital angular momentum. The small black hole is not spinning.

We expect this configuration to exhibit significant precession. The leading post-Newtonian contribution due to spin is the spin-orbit interaction, which can be characterized by the Hamiltonian [47] (see also, for example, Ref. [48])

$$H_{\rm SO} = 2\frac{\mathbf{S}_{\rm eff}\cdot\mathbf{L}}{r^3}, \tag{4.1}$$

where r is the coordinate separation of the black holes, and the effective spin $\mathbf{S}_{\rm eff}$ is defined as

$$\mathbf{S}_{\rm eff} = \left(1+\frac{3}{4}\frac{M_2}{M_1}\right)\mathbf{S}_1 + \left(1+\frac{3}{4}\frac{M_1}{M_2}\right)\mathbf{S}_2, \tag{4.2}$$

where in our case one of the spins would be zero. From the spin-orbit interaction one can derive a post-Newtonian evolution equation for the black-hole spin [47],

$$\dot{\mathbf{S}} = -\frac{2}{r^3}\mathbf{S}_{\rm eff} \times \mathbf{L}. \tag{4.3}$$

This indicates that the maximum amount of spin precession will be achieved when the spin is perpendicular to the orbital angular momentum. If one of the black holes has a Kerr parameter S_i/M_i^2, then S will be largest if the larger black hole is spinning. This is also convenient from a numerical point of view, because the resolution requirements increase both as the mass is decreased, and spin is added; it is computationally cheaper to put the spin on the larger black hole.

We also know from PN theory that $\dot{\mathbf{S}} = -\dot{\mathbf{L}}$ in the absence of gravitational radiation. If we increase the mass ratio, then the orbital angular momentum L at a given separation will decrease, but the magnitude of the spin will stay the same. Therefore the relative change in $\mathbf{L}$ due to the precession of the spins will increase. This means that we will get greater spin precession for higher mass ratios. We have chosen $q = 3$ because this is reasonably large compared to typical simulations we have performed in the past, but low enough that we still expect to be able to achieve high accuracy.

Figure 5 shows the orbital motion of the two punctures in the simulation. The precession of the orbital plane is clearly visible in the figure.

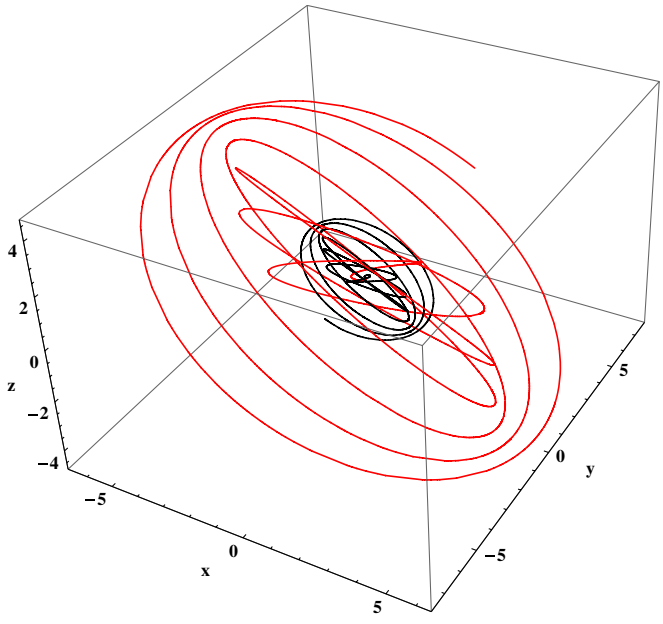

FIG. 5 (color online). Motion of the black-hole punctures for the $q = 3$ precession simulation. The motion of the small black hole is shown in red, and the large black hole is shown in black. The precession of the orbital plane is clearly visible through the inspiral.

Considering the leading order spin-orbit interaction Eq. (4.1) also exhibits another subtle feature of spinning binaries. The time evolution of the momentum vector $\mathbf{p}$ is given by the Hamiltonian evolution equation

$$\frac{d\mathbf{p}}{dt} = -\frac{\partial H}{\partial \mathbf{r}}. \tag{4.4}$$

If the Hamiltonian H depends on the spins, then consequently the momentum also picks up a contribution from the spins, and the velocity vector $\dot{\mathbf{r}}$ is in general *not* parallel to the momentum $\mathbf{p}$. Consequently, the directions of the orbital frequency vector Ω,

$$\Omega = \frac{\mathbf{r} \times \mathbf{v}}{r^2} \tag{4.5}$$

is in general *not* aligned with the angular momentum $\mathbf{L} = \mathbf{r} \times \mathbf{p}$. For the spin-orbit interaction defined by the Hamiltonian in Eq. (4.1), this contribution to the angular momentum can be computed as [47]

$$L_{\rm SO} = \frac{\mu}{M}\left[\frac{M}{r}\mathbf{n} \times \left(\mathbf{n} \times \left(3\mathbf{S} + \frac{\delta m}{M}\Delta\right)\right) - \frac{1}{2}\mathbf{v} \times \left(\mathbf{v} \times \left(\mathbf{S} + \frac{\delta m}{M}\Delta\right)\right)\right], \tag{4.6}$$

where

$$\Delta = M\left(\frac{\mathbf{S}_1}{M_2} - \frac{\mathbf{S}_2}{M_1}\right), \tag{4.7}$$

and $\mathbf{v} = \dot{\mathbf{r}}$, and $\mathbf{n}$ is the unit vector in the direction of $\mathbf{r}$. The total orbital angular momentum is then $L = L_{\rm NS} + L_{\rm SO}$, and $L_{\rm NS}$ is the nonspinning contribution to the angular momentum (which is parallel to the vector $\mathbf{r} \times \mathbf{v}$).

Note that the effect of the nonalignment of Ω and $\mathbf{L}$ is maximal when the spin $\mathbf{S}$ is in the orbital plane. This is indeed the case for our initial conditions, and also during the evolution the spin component out of the orbital plane is significantly smaller than the components in the orbital plane. Note also that since the spin typically varies on a timescale larger than the orbital time scale, Eq. (4.6) will lead to oscillations in the angle between Ω and $\mathbf{L}$ with roughly the orbital period.

Such oscillations are not present in the direction of $\mathbf{L}$, as illustrated in Fig. 6. We will see later that the quadrupole-aligned frame moves consistently with $\mathbf{L}$ (i.e., as a smooth function), suggesting that our maximization procedure tracks the direction of the orbital angular momentum.

The left panel of Fig. 7 shows the amplitude of the ($\ell = 2$, $m = 2$) and ($\ell = 2$, $m = 1$) modes during the inspiral. We clearly see that the "subdominant" (2, 1) mode is of comparable magnitude to the (2, 2) mode, and shows significant modulation. (It is also instructive to compare with the results in [49], where a precessing binary is also considered from a fixed frame of reference, and all of the $\ell = 2$ modes are of significant amplitude.) The right panel of Fig. 7 shows the frequency of the (2, 2) mode,

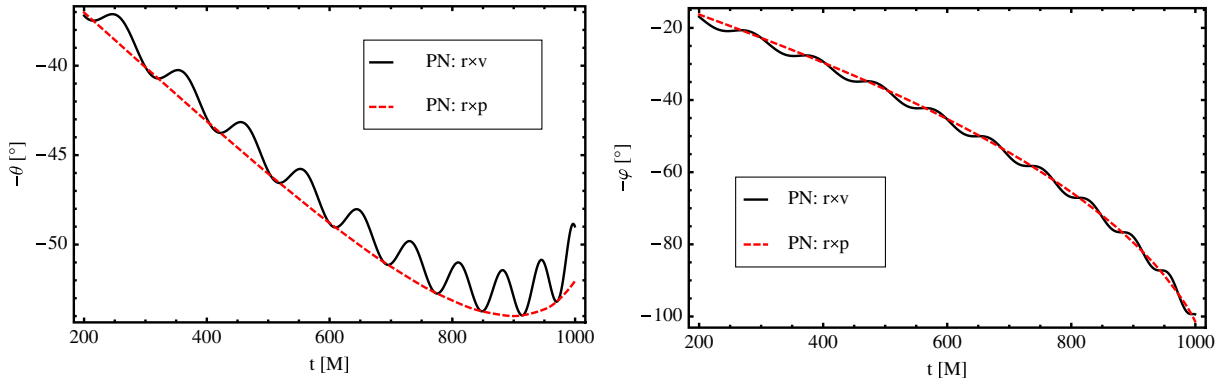

FIG. 6 (color online). Comparison of the polar angles θ and φ for the unit directions of $\mathbf{r} \times \mathbf{v}$ (normal to the orbital plane) and $\mathbf{r} \times \mathbf{p}$ (orbital angular momentum) in a PN calculation. The comparison shows that the direction of $\mathbf{r} \times \mathbf{v}$ exhibits extra oscillations.

$\omega_{22} = \dot{\varphi}_{22}$, over the same time interval. The frequency clearly exhibits large oscillations. Based on the discussion around Eq. (1.1) we expect oscillations in ω_{22} of purely physical origin, but we also assume that the physical oscillations will be exaggerated and their frequency modified in the fixed frame of an inertial observer.

We now apply the maximization procedure to the waveform signal from $t = 200M$, when the junk radiation has passed, through merger and ringdown (up to $t = 1350M$). At each time step the system is rotated such that the ($\ell = 2$, $|m| = 2$) mode amplitudes are maximized.

Having applied our maximization procedure to track the precession, we first address the question of whether the GW signal is emitted normal to the orbital plane, or parallel to the orbital angular momentum. Although we cannot unambiguously define the direction of orbital angular momentum, we can certainly determine whether the GW signal is emitted normal to the orbital plane.

Figure 8 shows the Euler angles (β, γ) that were found in the maximization procedure, time shifted by $103M$ to approximately compensate for the time lag to the extraction spheres. It also shows the angles (θ, φ) of the direction orthogonal to the orbital plane as computed from the NR simulation, and for the orbital angular momentum $\mathbf{L}$ as computed from a PN simulation (as in Fig. 6). The PN angles are approximately aligned with (β, γ) at early times. If the GW signal were emitted normal to the orbital plane, we would expect to be able to align β with $-\theta$ from the numerical relativity simulation, and likewise for γ and $-\varphi$. However, it is clear from Fig. 8 that the orbital-plane angles contain extra oscillations. Based on the illustration in Fig. 6, this suggests that the GW signal is emitted in the direction of the orbital angular momentum. In particular, we plot in Fig. 8 the direction of the orbital angular momentum as predicted in PN theory, which shows good agreement with the angles that define the quadrupole-aligned frame.

Figure 9 shows the amplitude of the original $\Psi'_{4,22}$ and the quadrupole-aligned signal that results from the maximization procedure, $\Psi_{4,22}$. We see that the maximization procedure has indeed increased the amplitude at all times, and also seems to have removed some oscillations.

The frequency of the ($\ell = 2$, $m = 2$) mode before and after the maximization procedure is shown in Fig. 10. This

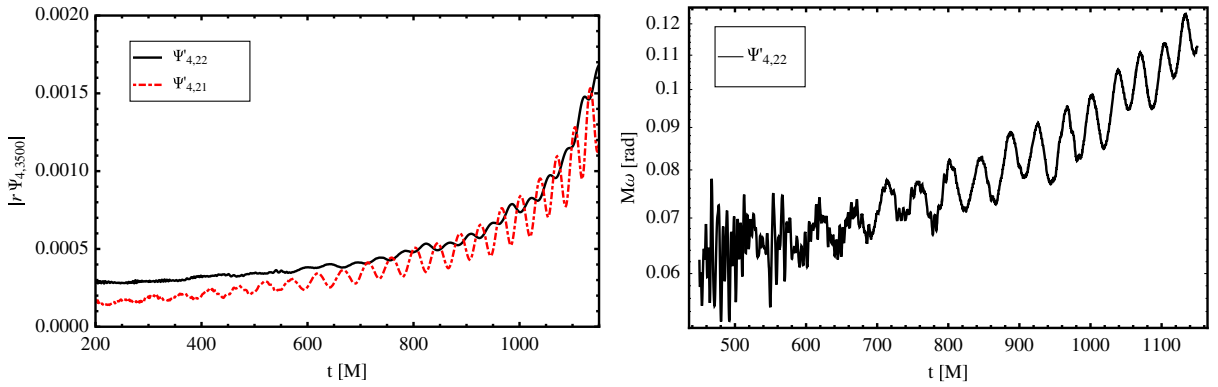

FIG. 7 (color online). Amplitude of raw numerical data for inspiral (left), for the "dominant" mode $\Psi'_{4,22}$ and the "subdominant" mode $\Psi'_{4,21}$. The right panel shows the frequency of the ($\ell = 2$, $m = 2$) mode, which exhibits significant oscillations. (The data are also noisy at early times, but this is typical for such data.)

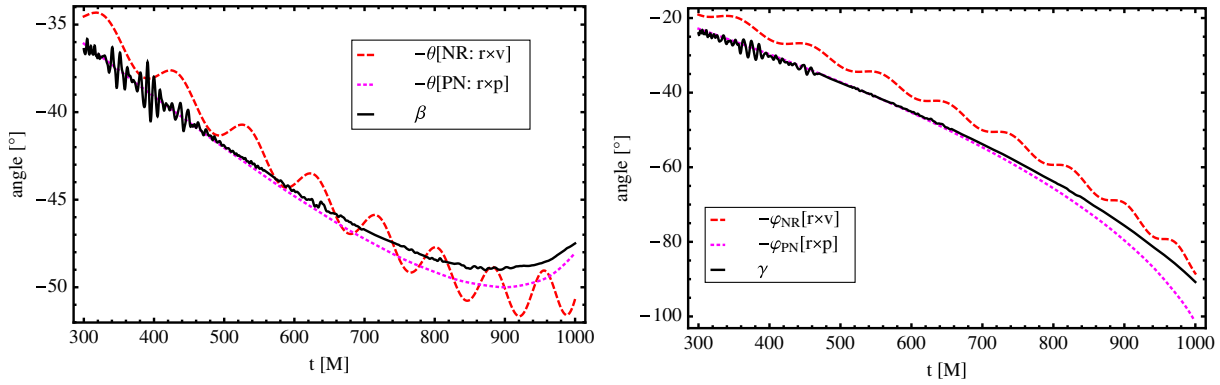

FIG. 8 (color online). The Euler angles (β, γ) found when the maximization procedure was applied to the $q = 3$ precessing-binary waveform. For comparison we show the corresponding angles $(-\theta, -\varphi)$ of the normal to the orbital plane as computed from the NR simulation, and for the angular momentum $\mathbf{L}$ from a PN simulation (as in Fig. 6). We approximately align the PN angles with β and γ at early times. We clearly see that the orbital-plane angles show additional oscillations that are not present in the (2, 2)-maximization angles.

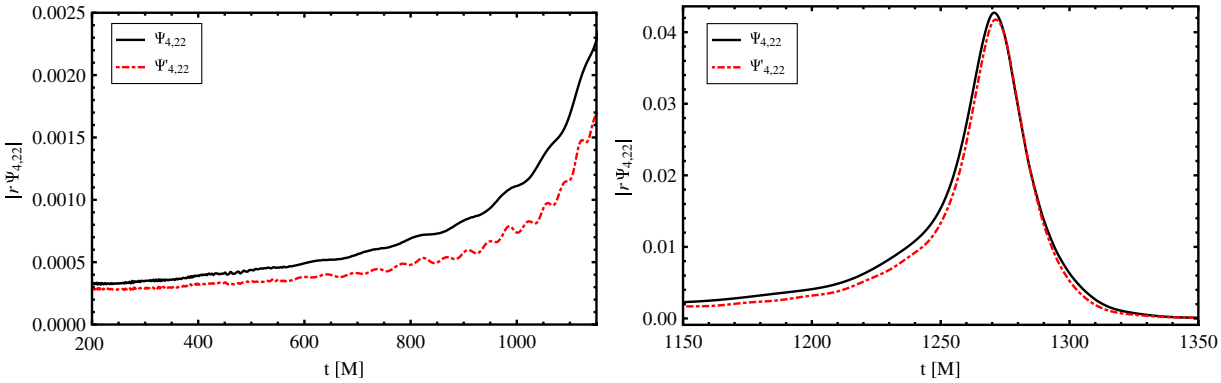

FIG. 9 (color online). Amplitude of the $(\ell = 2, m = 2)$ mode, before $(\Psi'_{4,22})$ and after $(\Psi_{4,22})$ the maximization procedure.

figure illustrates one of the key results of this work: the high-frequency oscillations in the wave frequency have been removed by the maximization procedure, and we are left with a far simpler functional form. We note,

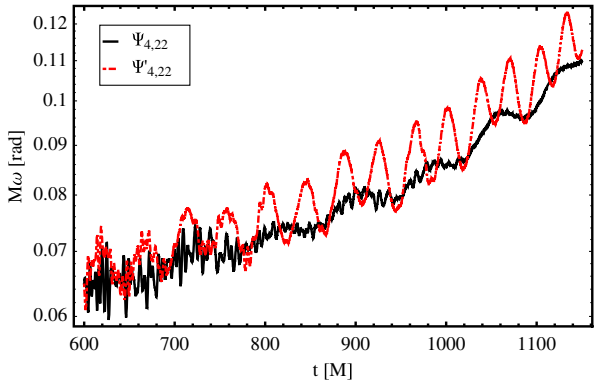

FIG. 10 (color online). Frequency of the $(\ell = 2, m = 2)$ mode before $(\Psi'_{4,22})$ and after $(\Psi_{4,22})$ the maximization procedure. We see that the high-frequency oscillations have been removed. The remaining oscillations are of a lower frequency and much lower amplitude; see text and Fig. 11.

however, that the oscillations in the frequency have not been completely removed. This is to be expected from Eq. (1.1). In the absence of precession, during the inspiral the gravitational-wave frequency of a spherical-harmonic mode (ℓ, m) is with a high degree of accuracy proportional to the orbital frequency, $\omega_{\ell m} = M\omega_{\rm orb}$. In the presence of precession, this is however replaced by Eq. (1.1), which adds an extra term depending on the precessing motion of the orbital plane. In Fig. 11 we compare the frequency of the $(\ell = 2, m = 2)$ mode after the maximization procedure with the orbital frequency with the precession term added according to Eq. (1.1), and we find reasonable agreement. We also show the frequency ω_N that results from rotating the system according to the direction perpendicular to the orbital plane, which is also the direction of the naive Newtonian orbital angular momentum. It is clear from Fig. 11 that the oscillations due to the orbital-plane rotations are much larger, and this further suggests that the quadrupole-aligned frame is optimal. We have also verified that the remaining oscillations are *not* due to residual eccentricity in the system, by repeating our analysis on a simulation with roughly twice the eccentricity, and by studying PN examples.

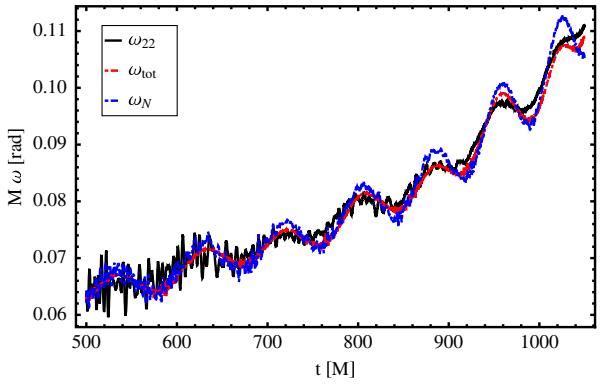

FIG. 11 (color online). Frequency of the ($\ell = 2$, $m = 2$) mode after ($\Psi_{4,22}$) the maximization procedure, compared with the "total frequency" $\omega_{\rm tot}$, which is the orbital frequency with a precession term added according to Eq. (1.1). We also show the frequency that results from rotating the system according to the direction of the Newtonian orbital angular momentum, ω_N, i.e., the normal to the orbital plane. The frequencies, in order of increasing magnitude of oscillation, are ω_{22}, $\omega_{\rm tot}$ and ω_N.

It is clear that the maximization procedure produces ($\ell = 2$, $|m| = 2$) modes that are of a simpler form than in the original data. However, this is not a guarantee that we have correctly tracked the direction of the GW emission; we have not necessarily put the waveform into a physically meaningful frame of reference. One test of our method is to calculate the effect on the subdominant modes. We expect that in the quadrupole-aligned frame the amplitude of the GW signal will agree to a good approximation with that from a $q = 3$ nonspinning binary. (The spin effect on the rate of inspiral is dominated by $\mathbf{S} \cdot \mathbf{L}$, and this is close to zero throughout our simulation, so we expect the inspiral to be similar to that for a nonspinning binary with the same mass ratio.)

Figure 12 shows a selection of modes for the quadrupole-aligned waveform. The left frame shows the transformed modes for the precessing binary, and the right frame shows the same modes for the nonspinning $q = 3$ waveform presented in [37]. Two things are remarkable about this figure. The first is that the amplitudes of the modes show extremely good agreement. The other is that we have found that the magnitude of the ($\ell = 2$, $m = 1$) mode is extremely sensitive to the angle by which the system is rotated. If, for example, we were to modify β or γ by a fraction of a degree, $\Psi_{4,21}$ could change by orders of magnitude. With this fact borne in mind, the oscillations in $|\Psi_{4,21}|$ are not very large at all. This figure suggests that we have located an optimal frame from which to study the GW signal.

Finally, we will discuss the application of our procedure to the merger and ringdown. We can calculate the final black hole's spin magnitude and direction using information from the apparent horizon [50]. Ideally our method would locate the same spin direction. However, as pointed out in Sec. IV A, the ringdown signal is a superposition of spheroidal (rather than spherical) harmonics [46,51], and so we do not expect a maximization of the $\ell = 2$, $|m| = 2$ coefficients of a spherical-harmonic decomposition of the waveform to necessarily produce meaningful results. And indeed, we find that our method does not locate the correct final-spin direction through ringdown. We intend to explore the use of spheroidal harmonics in future work.

V. DISCUSSION

We have presented a simple method to track the precession of a binary system, using only information from the GW signal. Our procedure is to rotate the system such that the magnitude of the ($\ell = 2$, $|m| = 2$) modes is maximized, based on the physical assumption that this will be the direction of dominant GW emission. We refer to this as the "quadrupole-aligned" waveform. Based on evidence from PN theory, we show that this direction seems to

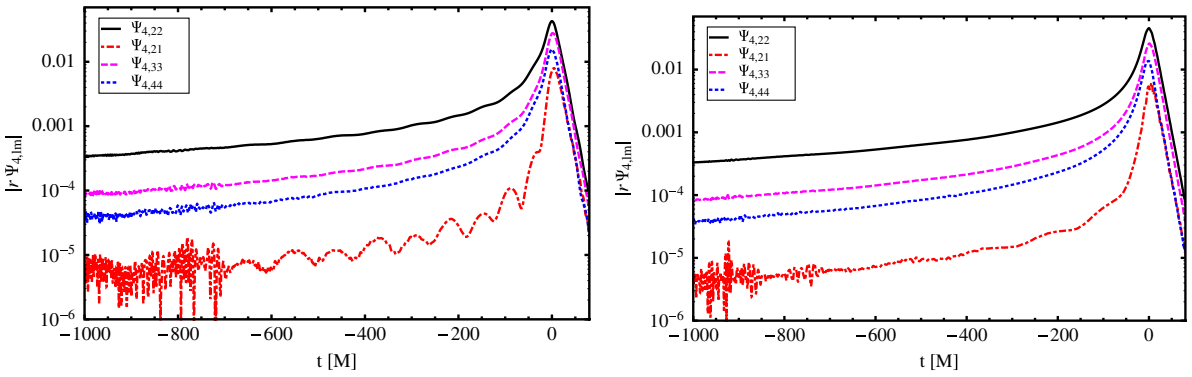

FIG. 12 (color online). Left: selected modes of the precessing-binary waveform, after being transformed into the nonprecessing frame, i.e., after the system has been rotated by the angles that were found from the (2, 2)-maximization procedure. The right-hand plot shows the same modes for a nonspinning (and therefore nonprecessing) $q = 3$ waveform. The agreement is remarkable. Note, in particular, the qualitative agreement of the ($\ell = 2$, $m = 1$) mode, which is of comparable magnitude to the ($\ell = 2$, $m = 2$) mode in the raw data (see Fig. 7).

correspond to that of the orbital angular momentum, which is in general *not* perpendicular to the orbital plane. We also show that our method produces higher-mode amplitudes consistent with what we know from comparable nonprecessing binaries.

The result of our procedure is that the waveform is represented in a more simple form than the one produced directly from the numerical code. This is particularly true for the subdominant modes; compare Figs. 7 and 12. We expect that this will simplify the task of producing analytic inspiral-merger-ringdown models, which is one of the main motivations for our work. This method also provides a *normal form* for the inspiral waveform, which will facilitate future comparisons between numerical and analytic results.

One could propose alternative procedures to track the precession of the system, and we will now discuss some of them, and their difficulties.

Only the total angular momentum of the spacetime is unambiguously defined in general relativity. The form of Bowen-York puncture initial data is such that we can analytically calculate the angular momentum ([29,52–54]) of the initial slice from the initial data parameters; it is simply given by $\mathbf{L} = \mathbf{r}_1 \times \mathbf{p}_1 + \mathbf{r}_2 \times \mathbf{p}_2$, where $\mathbf{r}_i$ are the coordinate locations of the punctures, and $\mathbf{p}_i$ are the momenta that are input into the Bowen-York extrinsic curvature. We can calculate the angular momentum radiated through the spheres on which we measure the GW signal, and so we can determine the total angular momentum of the system as a function of time. However, we want the *orbital* angular momentum, $\mathbf{L} = \mathbf{J} - \mathbf{S}$. To calculate this we need to know the black-hole spins as a function of time (which can be estimated with reasonable accuracy from the black holes' apparent horizons [50]), but these quantities are calculated at the black holes, not at the GW extraction sphere, and cannot easily be translated.

One could attempt to instead calculate the orbital angular momentum entirely at the sources, but this also presents difficulties. The proper distance between the black-hole horizons and their momenta could be calculated by some quasilocal procedure (for example [55]), and hence the orbital angular momentum. But it will be difficult to assess the gauge errors in any such method. Alternatively, one could calculate the angular momentum using the puncture locations and PN theory, but this will only be an approximation to the true general relativistic angular momentum. One direction we can easily determine is the normal to the orbital plane of the binary, but we have seen in Sec. IV, that this is not the direction in which the dominant GW signal is emitted, and nor does it define a reference frame from which the GW signal appears simpler than what can be achieved by the maximization procedure that we have used.

Nonetheless, a number of issues remain to be resolved in our procedure. In particular, our method does not seem to accurately track the quadrupole-aligned direction through merger and ringdown. If it were able to do this, it would provide an alternative procedure to determine the direction of the spin of the final black hole. We find that the angles from our maximization procedure continue to vary through merger and ringdown, and do not settle at constant values, which is what they would do if they corresponded to the final-spin direction. As we pointed out at the end of Sec. IV, this may be due to the decomposition of the waveform using an inappropriate basis; other subtle effects, for example, the motion of the center-of-mass of the system due to gravitational recoil, may also complicate the method. We will investigate these issues further in future work.

One may also question whether this method will work beyond the single precessing case that we have considered, which involved only one spinning black hole, and the spin direction was explicitly chosen such that $\mathbf{S} \cdot \mathbf{L} = 0$. However, we have made preliminary studies with a number of other precessing-binary configurations, and find results consistent with those presented here.

[While working on this project we have learned that an independent effort to identify precession effects via a similar algorithm will be presented by Seiler *et al.* in a forthcoming publication [56].]

ACKNOWLEDGMENTS

We thank Jennifer Seiler for letting us know about her ongoing work on a similar algorithm, and B. S. Sathyaprakash, Stephen Fairhurst, Michael Pürrer, and Denis Pollney for discussions. P. Schmidt is a recipient of a DOC-fFORTE-fellowship of the Austrian Academy of Sciences and was also partially supported by FWF grant P22498. M. Hannam was supported by FWF grant M1178 and Science and Technology Facilities Council grants ST/H008438/1 and ST/I001085/1. S. Husa was supported by grant FPA-2007-60220 from the Spanish Ministry of Science and the Spanish MICINNs Consolider-Ingenio 2010 Programme under grant MultiDark CSD2009-00064, and thanks Cardiff University for hospitality. P. Ajith was supported in part by NSF grants PHY-0653653 and PHY-0601459, and the David and Barbara Groce Fund at Caltech. BAM simulations were carried out at LRZ Munich, ICHEC Dublin, the Vienna Scientific Cluster (VSC), and at MareNostrum at Barcelona Supercomputing Center—Centro Nacional de Supercomputación (Spanish National Supercomputing Center).

APPENDIX: TRANSFORMATION OF $\Psi_{4,lm}$ UNDER ROTATIONS

We aim to derive the transformation of the Weyl scalar Ψ_4 under a rotation $\mathbf{R} \in SO(3)$. A similar calculation is performed in [49]. It can be shown that the Weyl scalar is a

field of spin-weight $s = -2$ and hence it can be expanded as

$$\Psi_4 = \sum_{l,m} \Psi_{4,lm} Y^{-2}_{lm}, \tag{A1}$$

where Y^{-2}_{lm} denote the spherical harmonics of spin-weight $s = -2$ [57]. For $s = 0$ we obtain the regular spherical harmonics Y_{lm}, which are the eigenfunctions of the angle-dependent part of the Laplace operator.

The transformation of the spin-weighted spherical harmonics is a simple composition of the transformation of the spin-basis-dependent part and of Y_{lm}. It is convenient to introduce standard polar coordinates (r, θ, φ) and to define Y_{lm} with respect to the polar angles (θ, φ). The spherical harmonics then have the form

$$Y_{lm}(\theta, \varphi) = \phi(\varphi)\Theta(\theta). \tag{A2}$$

We will consider rotations $\mathbf{R}$, which transform angles $\Omega = (\theta, \varphi)$ to the new coordinates $\Omega' = (\theta', \varphi')$. The spin-weight-zero spherical harmonics Y_{lm} then transform according to $Y_{lm}(\theta, \varphi) \mapsto Y_{lm}(\theta', \varphi')$ by applying the operator $\mathbf{P}_R$, where R is a rotation about the z-axis by the angle γ such that $\varphi \mapsto \varphi' = \varphi + \gamma$ and $\theta = \theta'$, is given by

$$Y_{lm}(\theta', \varphi') \equiv \mathbf{P}_R Y_{lm}(\theta, \varphi) = e^{im\gamma} Y_{lm}(\theta, \varphi). \tag{A3}$$

Now, let $\mathbf{R}(\gamma\beta\alpha)$ denote an arbitrary rotation by the Euler angles γ, β, α. Using the z-y-z convention, the spherical harmonics then obey the following transformation law [58,59]:

$$Y_{lm}(\theta', \varphi') = \sum_{m'=-l}^{l} e^{im'\gamma} d^l_{m'm}(\beta) e^{im\alpha} Y_{lm}(\theta, \varphi), \tag{A4}$$

where the $d^l_{m'm}$ denote the Wigner d-matrices which are given by [60]

$$\begin{aligned} d^l_{m'm} = {} & \sqrt{(l+m)!(l-m)!(l+m')!(l-m')!} \\ & \times \sum_k \frac{(-1)^{k+m'-m}}{k!(l+m-k)!(l-m'-k)!(m'-m+k)!} \\ & \times \left(\sin\frac{\beta}{2}\right)^{2k+m'-m} \left(\cos\frac{\beta}{2}\right)^{2l-2k-m'+m}. \end{aligned} \tag{A5}$$

Because of the properties of the group $SO(3)$, the inverse transformation is then given by

$$Y_{lm}(\theta, \varphi) = \sum_{m'=-l}^{l} e^{-im'\gamma} d^l_{m'm}(-\beta) e^{-im\alpha} Y_{lm'}(\theta', \varphi'). \tag{A6}$$

The next step is to include the change of spin basis under a rotation. According to [61] a quantity η of spin-weight s obeys the following law under a change of the spin basis:

$$\eta' = \eta e^{is\chi}. \tag{A7}$$

Combining Eqs. (A6) and (A7) yields the transformation law for the spin-weighted spherical harmonics:

$$Y^s_{lm}(\theta, \varphi) = e^{-is\chi} \sum_{m'=-l}^{l} e^{-im'\gamma} d^l_{m'm}(-\beta) e^{-im\alpha} Y^s_{lm'}(\theta', \varphi'). \tag{A8}$$

We invert Eq. (A1) to determine the transformation law for the $\Psi_{4,lm}$-modes,

$$\begin{aligned} \Psi_{4,lm} = {} & \int \Psi_4 \overline{Y^s_{lm}(\theta, \varphi)} d\Omega \\ = {} & \int e^{-is\chi} \Psi'_4 e^{is\chi} \sum_{m'} e^{im'\gamma} d^l_{m'm}(-\beta) \\ & \times e^{im\alpha} \overline{Y^s_{lm'}(\theta', \varphi')} d\Omega' \\ = {} & \sum_{m'=-l}^{l} e^{im'\gamma} d^l_{m'm}(-\beta) e^{im\alpha} \Psi'_{4,lm'}, \end{aligned} \tag{A9}$$

where we see that explicit knowledge of χ as a function of θ and φ is not necessary to determine the coefficients $\Psi_{4,\ell m}$. This transformation law can now be applied to any given $\Psi'_{4,lm}$, e.g., our numerical data, in order to change the frame of reference. The remaining free parameters are the three angles that determine the general rotation. In practice, one does not need to perform the third rotation about α [49,58]. We therefore restrict ourselves to a rotation about two the Euler angles, β and γ, only. Since we aim to align the orbital angular momentum with the z-axis at every instant of time, i.e., $\hat{L} \mapsto \hat{z}$, a simple calculation shows that in order to fulfill this $\beta = -\theta$ and $\gamma = -\varphi$ are required, where (θ, φ) are the polar coordinates determining the direction of $\hat{L}$.

[1] B. S. Sathyaprakash and B. F. Schutz, Living Rev. Relativity **12**, 2 (2009), http://www.livingreviews.org/lrr-2009-2.

[2] L. Blanchet, Living Rev. Relativity **9**, 4 (2006), http://www.livingreviews.org/lrr-2006-4.

[3] T. Damour and A. Nagar, arXiv:0906.1769.

[4] F. Pretorius, Phys. Rev. Lett. **95**, 121101 (2005).

[5] M. Campanelli, C. O. Lousto, P. Marronetti, and Y. Zlochower, Phys. Rev. Lett. **96**, 111101 (2006).

[6] J. G. Baker, J. Centrella, D.-I. Choi, M. Koppitz, and J. van Meter, Phys. Rev. Lett. **96**, 111102 (2006).

[7] J. M. Centrella, J. G. Baker, B. J. Kelly, and J. R. van Meter, Rev. Mod. Phys. **82**, 3069 (2010).

[8] P. Ajith *et al.*, Class. Quant. Grav. **24**, S689 (2007).

[9] P. Ajith *et al.*, Phys. Rev. D **77**, 104017 (2008).
[10] P. Ajith, Classical Quantum Gravity **25**, 114033 (2008).
[11] A. Buonanno *et al.*, Phys. Rev. D **76**, 104049 (2007).
[12] T. Damour and A. Nagar, Phys. Rev. D **77**, 024043 (2008).
[13] T. Damour, A. Nagar, E. N. Dorband, D. Pollney, and L. Rezzolla, Phys. Rev. D **77**, 084017 (2008).
[14] T. Damour, A. Nagar, M. Hannam, S. Husa, and B. Brügmann, Phys. Rev. D **78**, 044039 (2008).
[15] J. G. Baker *et al.*, Phys. Rev. D **78**, 044046 (2008).
[16] A. H. Mroue, L. E. Kidder, and S. A. Teukolsky, Phys. Rev. D **78**, 044004 (2008).
[17] T. Damour and A. Nagar, Phys. Rev. D **79**, 081503 (2009).
[18] A. Buonanno *et al.*, Phys. Rev. D **79**, 124028 (2009).
[19] P. Ajith *et al.*, Phys. Rev. Lett. **106**, 241101 (2011).
[20] L. Santamaría *et al.*, Phys. Rev. D **82**, 064016 (2010).
[21] Y. Pan *et al.*, Phys. Rev. D **81**, 084041 (2010).
[22] R. Sturani, S. Fischetti, L. Cadonati, G. Guidi, J. Healy *et al.*, J. Phys. Conf. Ser. **243**, 012007 (2010).
[23] J. G. Baker, M. Campanelli, F. Pretorius, and Y. Zlochower, Classical Quantum Gravity **24**, S25 (2007).
[24] Y. Pan *et al.*, Phys. Rev. D **77**, 024014 (2008).
[25] M. Hannam *et al.*, Phys. Rev. D **79**, 084025 (2009).
[26] M. Favata, Astrophys. J. **696**, L159 (2009).
[27] D. Pollney and C. Reisswig, arXiv:1004.4209.
[28] K. Arun, A. Buonanno, G. Faye, and E. Ochsner, Phys. Rev. D **79**, 104023 (2009).
[29] B. Brügmann *et al.*, Phys. Rev. D **77**, 024027 (2008).
[30] S. Husa, J. A. González, M. Hannam, B. Brügmann, and U. Sperhake, Class. Quant. Grav. **25**, 105006 (2008).
[31] S. Brandt and B. Brügmann, Phys. Rev. Lett. **78**, 3606 (1997).
[32] J. M. Bowen and J. W. York, Jr., Phys. Rev. D **21**, 2047 (1980).
[33] M. Ansorg, B. Brügmann, and W. Tichy, Phys. Rev. D **70**, 064011 (2004).
[34] M. Hannam, S. Husa, D. Pollney, B. Brügmann, and N. Ó Murchadha, Phys. Rev. Lett. **99**, 241102 (2007).
[35] M. Shibata and T. Nakamura, Phys. Rev. D **52**, 5428 (1995).
[36] T. W. Baumgarte and S. L. Shapiro, Phys. Rev. D **59**, 024007 (1998).
[37] M. Hannam, S. Husa, F. Ohme, D. Muller, and B. Bruegmann, Phys. Rev. D **82**, 124008 (2010).
[38] M. Hannam, S. Husa, and N. Ó Murchadha, Phys. Rev. D **80**, 124007 (2009).
[39] S. Husa, M. Hannam, J. A. González, U. Sperhake, and B. Brügmann, Phys. Rev. D **77**, 044037 (2008).
[40] A. Gopakumar, M. Hannam, S. Husa, and B. Brügmann, Phys. Rev. D **78**, 064026 (2008).
[41] M. Hannam, S. Husa, B. Brügmann, and A. Gopakumar, Phys. Rev. D **78**, 104007 (2008).
[42] A. H. Mroue, H. P. Pfeiffer, L. E. Kidder, and S. A. Teukolsky, Phys. Rev. D **82**, 124016 (2010).
[43] A. Buonanno, L. E. Kidder, A. H. Mroue, H. P. Pfeiffer, and A. Taracchini, Phys. Rev. D **83**, 104034 (2011).
[44] M. Hannam, S. Husa, U. Sperhake, B. Brügmann, and J. A. González, Phys. Rev. D **77**, 044020 (2008).
[45] M. Pürrer, S. Husa, and M. Hannam (unpublished).
[46] S. A. Teukolsky, Astrophys. J. **185**, 635 (1973).
[47] L. E. Kidder, Phys. Rev. D **52**, 821 (1995).
[48] A. Buonanno, Y. Chen, and T. Damour, Phys. Rev. D **74**, 104005 (2006).
[49] M. Campanelli, C. O. Lousto, H. Nakano, and Y. Zlochower, Phys. Rev. D **79**, 084010 (2009).
[50] M. Campanelli, C. O. Lousto, Y. Zlochower, B. Krishnan, and D. Merritt, Phys. Rev. D **75**, 064030 (2007).
[51] R. A. Breuer, M. P. Ryan Jr., and S. Waller, Proc. R. Soc. A **358**, 71 (1977).
[52] N. Ó Murchadha and J. W. York, Jr., Phys. Rev. D **10**, 428 (1974).
[53] J. W. York, Jr., Ann. Inst. Henri Poincaré **21**, 319 (1974).
[54] J. W. York, in *Sources of Gravitational Radiation*, edited by L. L. Smarr (Cambridge University Press, Cambridge, UK, 1979), pp. 83–126, ISBN .
[55] B. Krishnan, C. O. Lousto, and Y. Zlochower, Phys. Rev. D **76**, 081501 (2007).
[56] J. Seiler *et al.* (unpublished).
[57] E. T. Newman and R. Penrose, J. Math. Phys. (N.Y.) **7**, 863 (1966).
[58] E. P. Wigner, *Group Theory and its Application to the Quantum Mechanics of Atomic Spectra* (Academic Press Inc., New York, 1959), ISBN .
[59] J. N. Goldberg, A. J. MacFarlane, E. T. Newman, F. Rohrlich, and E. C. G. Sudarshan, J. Math. Phys. (N.Y.) **8**, 2155 (1967).
[60] J. J. Sakurai, *Modern Quantum Mechanics* (Addison-Wesley Publishing Company, Reading, MA, 1994), revised ed., ISBN .
[61] M. Alcubierre, *Introduction to* 3 + 1 *Numerical Relativity* (Oxford University Press, New York, 2008), ISBN .